Climate effects of high-latitude volcanic eruptions: Role of the time of year

Ben Kravitz[1] and Alan Robock[1]

Received 4 May 2010; revised 20 September 2010; accepted 5 October 2010; published 7 January 2011.

[1] We test how the time of year of a large Arctic volcanic eruption determines the climate impacts by conducting simulations with a general circulation model of Earth's climate. For eruptions injecting less than about 3 Tg of SO_2 into the lower stratosphere, we expect no detectable climatic effect, no matter what the season of the eruption. For an injection of 5 Tg of SO_2 into the lower stratosphere, an eruption in the summer would cause detectable climate effects, whereas an eruption at other times of the year would cause negligible effects. This is mainly due to the seasonal variation in insolation patterns and sulfate aerosol deposition rates. In all cases, the sulfate aerosols that form get removed from the atmosphere within a year after the eruption by large-scale deposition. Our simulations of a June eruption have many similar features to previous simulations of the eruption of Katmai in 1912, including some amount of cooling over Northern Hemisphere continents in the summer of the eruption, which is an expected climate response to large eruptions. Previous Katmai simulations show a stronger climate response, which we attribute to differences in choices of climate model configurations, including their specification of sea surface temperatures rather than the use of a dynamic ocean model as in the current simulations.

Citation: Kravitz, B., and A. Robock (2011), Climate effects of high-latitude volcanic eruptions: Role of the time of year, *J. Geophys. Res.*, *116*, D01105, doi:10.1029/2010JD014448.

1. Introduction

[2] The past 2 years have seen significant volcanic activity, most notably the two large eruptions of Kasatochi (52.1°N, 175.3°W) on 8 August 2008 and Sarychev (48.1°N, 153.2°E) on 12 June 2009. Each injected between 1 and 2 Tg of SO_2 into the lower stratosphere [*Haywood et al.*, 2010; *Corradini et al.*, 2010; S. Carn, NASA Earth Observatory, Sulfur dioxide cloud from Aleutians' Kasatochi Volcano, 2008, available at http://earthobservatory.nasa.gov/images/imagerecords/8000/8998/kasatochi_OMI_2008aug11_lrg.jpg], making them the largest volcanic eruptions since Mount Pinatubo and Mount Hudson in 1991 (S. Carn and A. Krueger, TOMS Volcanic Emissions Group, 2004, available at http://toms.umbc.edu/Images/Mainpage/toms_so2chart_color.jpg).

[3] Sulfate aerosols, formed from the oxidation of SO_2, have a long atmospheric lifetime in the stratosphere of 1–3 years, if injected in the tropics [*Budyko*, 1977; *Stenchikov et al.*, 1998]. They efficiently backscatter shortwave radiation, effectively increasing the planetary albedo for the lifetime of the aerosols [*Robock*, 2000]. This results in the primary climate effect of large volcanic eruptions, which is cooling of the surface and the troposphere during the boreal summer. Since sulfate aerosols are not perfect scatterers, the stratosphere warms after a large eruption [*Stenchikov et al.*, 1998], which can result in dynamical effects due to the alteration of the thermal profile of the lower and middle atmosphere. For large tropical eruptions, these effects include warming over the Northern Hemisphere continents during the boreal winter and a positive mode of the Arctic Oscillation [*Robock*, 2000, 2003; *Stenchikov et al.*, 2002, 2004].

[4] Additionally, large volcanic eruptions cause significant perturbations to the hydrological cycle [*Trenberth and Dai*, 2007]. This mostly manifests itself as a reduction of the Indian-African-Asian monsoon, due to differentially reduced solar flux over the Indian Ocean and the large landmasses of Asia and Africa [*Kravitz et al.*, 2010a]. This effect is magnified for high-latitude eruptions, and evidence of it has been seen in past proxy records and climate simulations of the eruptions of Laki in 1783–1784 at 68°N [*Thordarson and Self*, 2003; *Oman et al.*, 2006a] and Katmai on 6 June 1912 at 58°N [*Oman et al.*, 2005, 2006b].

[5] Despite the large amount of atmospheric SO_2 loading, the eruption of Kasatochi had little to no climate response [*Kravitz et al.*, 2010a], and we expect the same findings for Sarychev. We postulate that this is due to an insufficient amount of SO_2, despite being relatively large eruptions. *Kravitz et al.* [2010a] performed additional climate model simulations involving a 5 Tg eruption on 8 August, but still no climate effects were observed. This is puzzling, since 5 Tg of SO_2 is known to be sufficient to cause climate perturba-

[1]Department of Environmental Sciences, Rutgers University, New Brunswick, New Jersey, USA.

0148-0227/11/2010JD014448

Table 1. Specifications for the Ensembles Used in This Experiment[a]

Ensemble	Date of Injection	Approximate Season	Magnitude
Sarychev	12 June 2008	Summer	1.5 Tg SO_2
2 × Sarychev	12 June 2008	Summer	3 Tg SO_2
June (also Katmai)	12 June 2008	Summer	5 Tg SO_2
Kasatochi	8 August 2008	Autumn	1.5 Tg SO_2
2 × Kasatochi	8 August 2008	Autumn	3 Tg SO_2
August	8 August 2008	Autumn	5 Tg SO_2
March	1 March 2008	Spring	5 Tg SO_2
December	1 December 2007	Winter	5 Tg SO_2

[a]All ensembles have 20 members. Each ensemble is described by the time of year and amount of injection of SO_2 into the lower stratosphere of one grid box centered at 48°N, 172.5°W. The 1.5 Tg injections simulate the volcanic eruptions of Sarychev (12 June 2009) and Kasatochi (8 August 2008).

tions, specifically the eruption of Katmai on 6 June 1912 [*Oman et al.*, 2005]. Thus, we conjecture that the time of year of a large eruption plays a critical role in determining whether it will have a climate impact.

[6] Our primary goal in this paper is to assess the role the time of year of a high-latitude eruption will have on the climate effects. Specifically, we compare sulfate aerosol optical depth and radiative forcing from each of the simulated eruptions. We also evaluate the temperature and precipitation effects by comparing model results against natural variability as calculated by the model and observed in the real world. Additionally, we compare our simulation of a 5 Tg eruption in June to the simulation of Katmai by *Oman et al.* [2005].

2. Experiment

[7] We simulated the climate response to high-latitude volcanic eruptions with ModelE, a coupled atmosphere-ocean general circulation model developed by the National Aeronautics and Space Administration Goddard Institute for Space Studies [*Schmidt et al.*, 2006]. We used the stratospheric version with 4° latitude by 5° longitude horizontal resolution and 23 vertical levels up to 80 km. It is fully coupled to a 4° latitude by 5° longitude dynamic ocean with 13 vertical levels [*Russell et al.*, 1995]. The aerosol module [*Koch et al.*, 2006] accounts for SO_2 conversion to sulfate aerosols, hydration of the aerosols from a specified dry radius of 0.25 μm, based on formulas by *Tang* [1996], and transport and removal of the aerosols. Radiative forcing (called "adjusted forcing" by *Intergovernmental Panel on Climate Change* (*IPCC*) [2001] and *Hansen et al.* [2005])

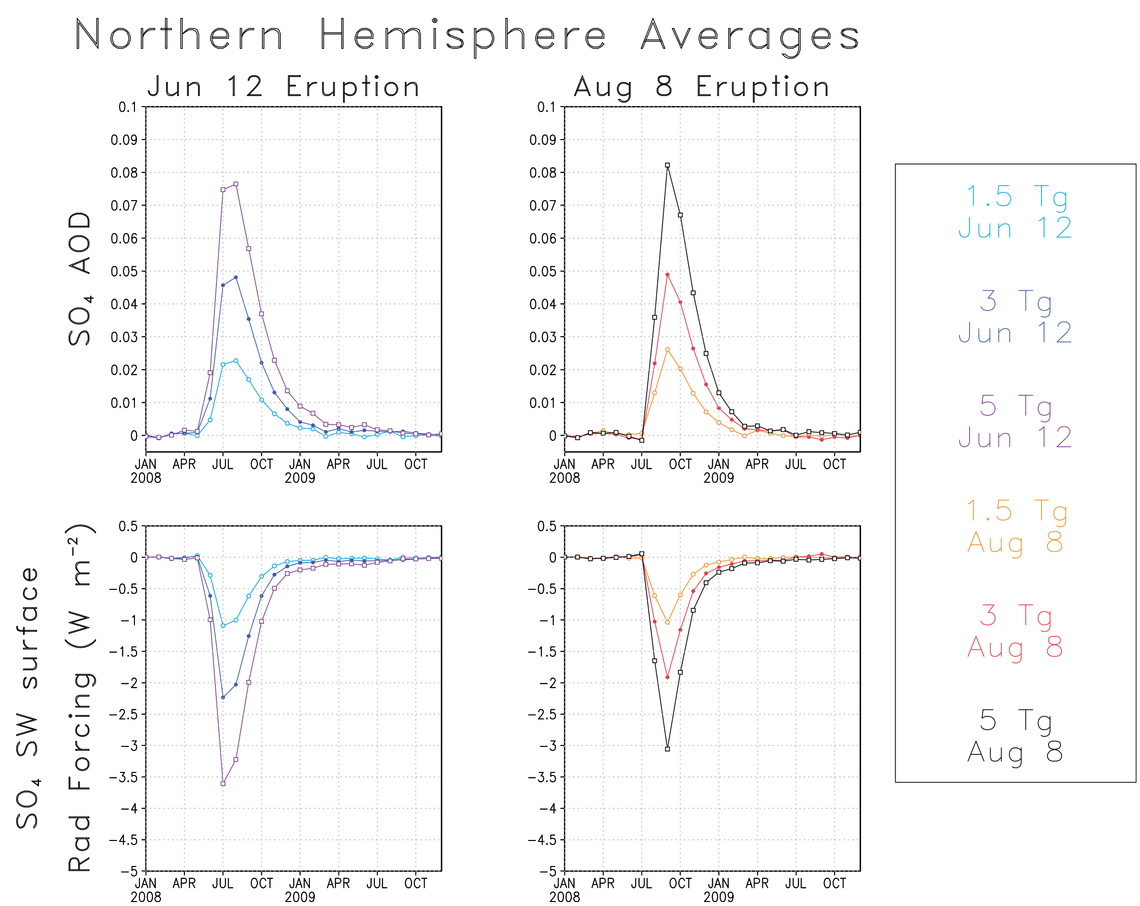

Figure 1. Northern Hemisphere averages for the June and August ensembles of sulfate aerosol optical depth and shortwave radiative forcing at the surface due to sulfate aerosols. All ensembles pictured are averages of 20 model runs. All values fall to very small amounts by the spring following the eruption and return to background levels within a year after the eruption.

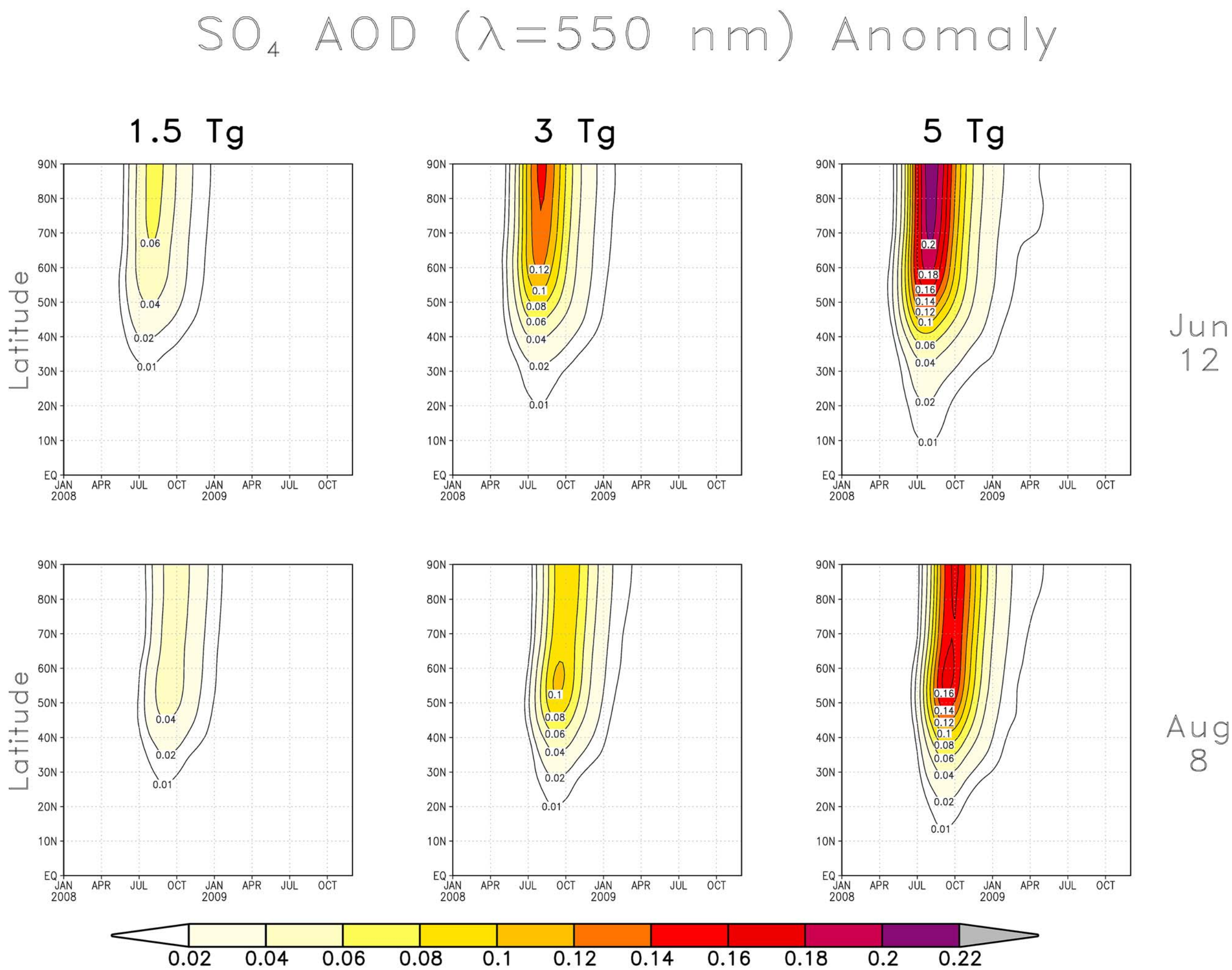

Figure 2. Zonally averaged sulfate aerosol optical depth (midvisible, λ = 550 nm) for the June and August ensembles. All ensembles pictured are averages of 20 model runs. Only the Northern Hemisphere is shown, as all values are zero in the Southern Hemisphere.

is fully interactive with the atmospheric circulation. For further details, see *Kravitz et al.* [2010a], who use the same model setup.

[8] Our control ensemble was a 20-member ensemble of 4 year runs (2007–2010), during which greenhouse gas concentrations increased according to the Intergovernmental Panel on Climate Change's A1B scenario [*IPCC*, 2007]. Testing the model by conducting simulations of constant 2007 greenhouse gas and aerosol concentrations gives no detectable temperature trend for the period 2007–2010, which is the period over which our simulations have been conducted.

[9] To examine the effects of the volcanic eruptions, we used six 20-member ensembles of 4 year simulations covering the same time period (Table 1). In these simulations, greenhouse gas concentrations increased in the same manner as in the control runs. We also injected SO_2 into the grid box centered at 52°N, 172.5°W, distributed equally in the three model layers that cover an altitude of 10–16 km. Three ensembles had an injection on 12 June 2008, and three had an injection on 8 August 2008, in the amounts of 1.5, 3, and 5 Tg of SO_2. The 1.5 Tg injections are meant to simulate the eruptions of Sarychev and Kasatochi. Although the eruption of Sarychev occurred in 2009 instead of 2008, we chose to simulate this 1.5 Tg injection in 2008 for the sake of comparison. The model does not show any significant climatological differences between 2008 and 2009, so this change should not impact our results. The 3 and 5 Tg injections were included as part of a sensitivity study, although the 5 Tg June eruption is comparable to the eruption of Katmai on 6 June 1912. In section 5, we perform such a comparison between our simulations of a June eruption and a set of simulations of Katmai, which were performed for *Oman et al.* [2005].

[10] To complete the assessment of the role of the time of year, we performed two additional ensembles of 20 members each. The 12 June ensembles had SO_2 injections near the beginning of summer (1 June), and the 8 August ensembles had injections near the beginning of autumn (1 September). Therefore, our two new simulations involved injections on 1 December 2007 and 1 March 2008, which corresponds to the beginning of winter and spring, respec-

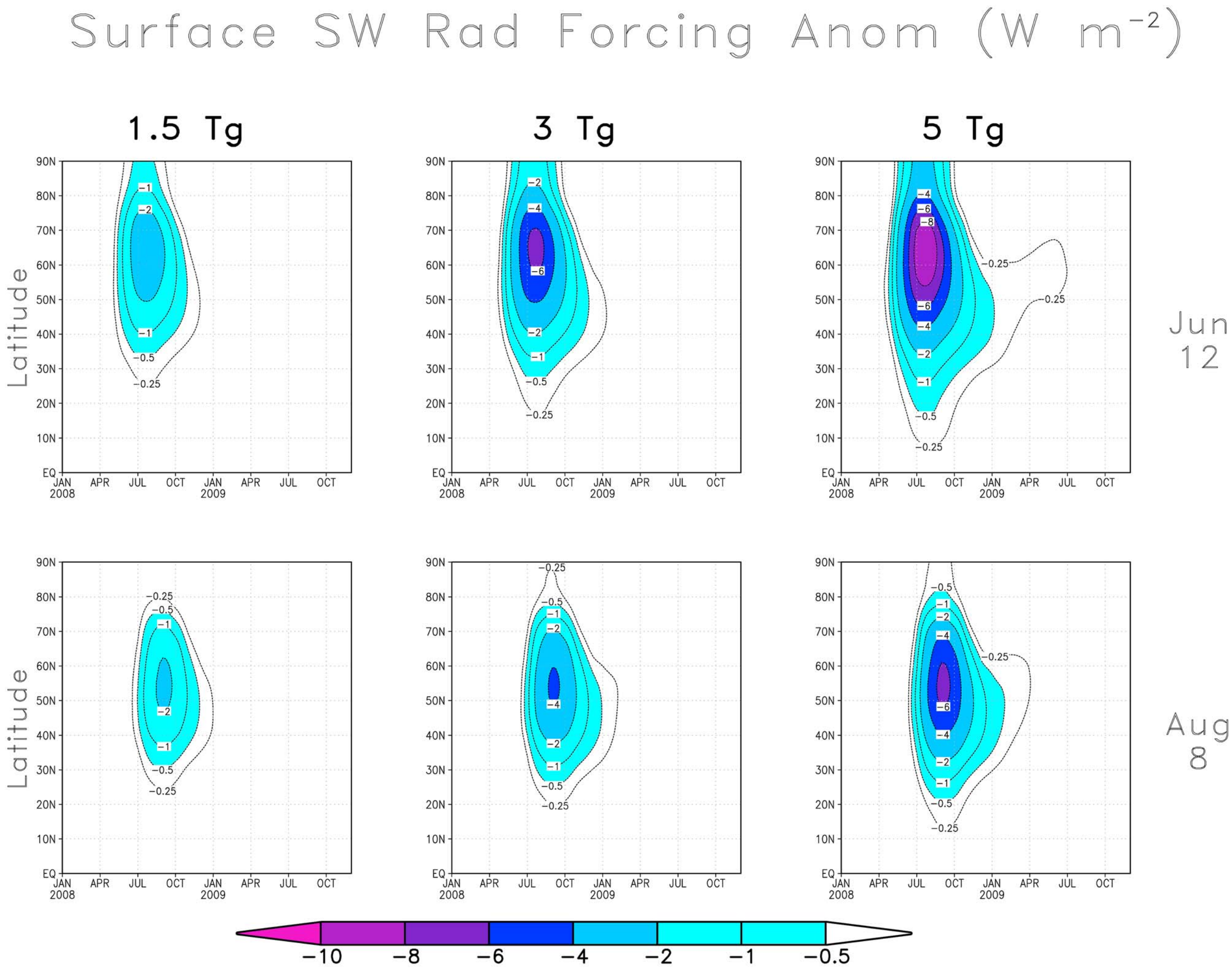

Figure 3. Zonally averaged surface shortwave radiative forcing (W m^{-2}) due to sulfate aerosols for the June and August ensembles. All ensembles pictured are averages of 20 model runs. Only the Northern Hemisphere is shown, as all values are zero in the Southern Hemisphere.

tively. Each ensemble member was a 3 year simulation (2007–2009) and involved an injection in the same grid box as the previous ensembles of 5 Tg SO_2. We only performed 3 year simulations, as prior analysis showed including the year 2010 did not give particularly interesting results.

[11] For their simulations of the 1912 eruption of Katmai, *Oman et al.* [2005] correlated their modeling results with data that showed a climate response to the eruption. This agreement between the model and observations or proxy records has also been verified for the eruptions of Laki in 1783–1784 [*Oman et al.*, 2006a, 2006b] and Pinatubo in 1991 [*Robock et al.*, 2007]. Therefore, we are confident in the model's ability to give us a realistic assessment of large-scale climate perturbations from volcanic eruptions.

3. Optical Depth and Radiative Forcing

[12] *Kravitz et al.* [2010a] analyzed both the modeled and observed climate impacts of the eruption of Kasatochi and determined such impacts were negligible. Preliminary analysis (not pictured) shows the same results for Sarychev. We conclude that a high-latitude volcanic eruption that injects 1.5 Tg of SO_2 into the lower stratosphere is of insufficient magnitude to cause significant climate impacts.

[13] To test our hypothesis that the time of year is important in determining whether a high-latitude eruption will have climate impacts, we wanted to simulate volcanic eruptions of a magnitude that is known to cause a detectable climate perturbation in both model studies and observations. Therefore, we chose to simulate a volcanic eruption that injected 5 Tg of SO_2 into the lower stratosphere, as this was the atmospheric loading due to Katmai.

[14] Figure 1 shows a comparison of Northern Hemisphere averaged aerosol optical depth (midvisible, λ = 550 nm) and shortwave radiative forcing at the surface due to the sulfate aerosols for the June and August climate model simulation ensembles. As expected, aerosol optical depth and radiative forcing both increase approximately linearly with increased atmospheric loading of SO_2. Also, aerosol optical depth drops to low levels (below 0.01) well before the spring after the eruption.

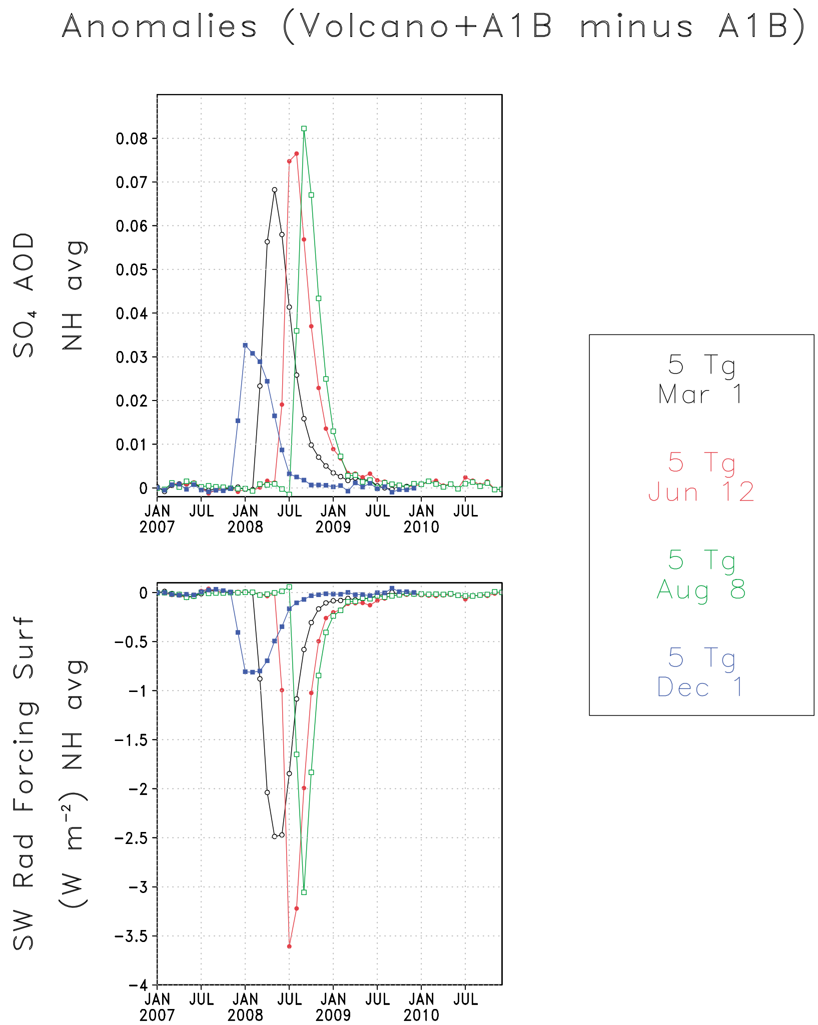

Figure 4. Same as Figure 1 for the 5 Tg ensembles. Integrating over the curves shown in the bottom from January 2007 to December 2010 yields values (in 10^{10} J m^{-2}) of −3.95 (March), −4.13 (June), −2.83 (August), and −2.36 (December).

Radiative forcing drops to low levels (smaller in magnitude than −0.25 W m^{-2}) at approximately the same time. The June eruptions reach larger peak radiative forcing than do the August eruptions, which is due to the much larger value of insolation affected by the June eruption than the August eruption, as is seen in Figure 7. The peak values of aerosol optical depth are comparable, regardless of the time of the eruption. All values of aerosol optical depth and radiative forcing return to background levels within a year after the eruptions.

[15] Figures 2 and 3 show the same results in more detail. We see in Figure 2 that although the bulk of the aerosol layer stays north of 30°N in latitude, the magnitude of the eruption correlates with the maximum latitudinal extent of the aerosol plume, i.e., the plumes from the larger eruptions reach farther south. The 5 Tg eruptions show a small amount of aerosols reaching the tropics. They also show evidence that some of the aerosols persisted through the winter into the following spring. Despite showing similar values of optical depth in both the June and August eruptions, Figure 3 shows the June ensembles generally have larger peaks of radiative forcing. The combination of different amounts of aerosol and latitudinal distribution of insolation results in a peak radiative forcing approximately 10° in latitude farther north for the June ensembles than the August ensembles. In all cases, aerosol optical depth and radiative forcing are at or near background levels 1 year after the eruptions and much sooner for all but the 5 Tg June 12 ensemble.

[16] Figures 4–6 show a similar analysis but for all of the 5 Tg ensembles. As we see in Figure 4, the March, June, and August eruptions all reach very similar peaks of aerosol optical depth, with the August ensemble showing the largest. However, the distribution of insolation is such that the June eruption has the largest peak radiative forcing. Figure 7 shows the average climatology of incident solar radiation at the surface, as well as the change in this field due to each of the 5 Tg volcanic eruptions. The largest reduction in insolation occurs for the March eruption, followed by the June, and then the August eruption. From Figure 4, optical depth from the March eruption peaks in June, which is the time of maximum insolation. Although optical depth is slightly higher for the June eruption, the peak occurs later, meaning

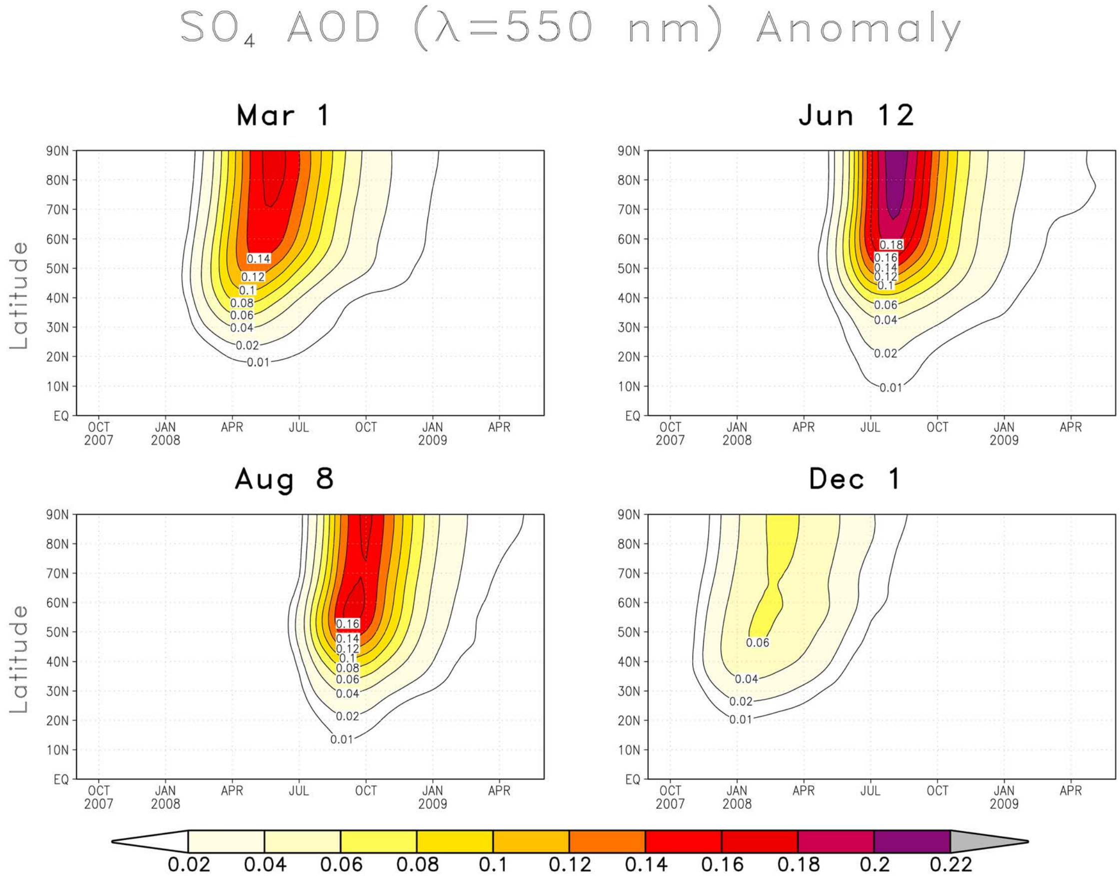

Figure 5. Zonally averaged sulfate aerosol optical depth (midvisible, $\lambda = 550$ nm) for the four ensembles for 5 Tg injections. All ensembles pictured are averages of 20 model runs. Only the Northern Hemisphere is shown, as all values are zero in the Southern Hemisphere. Top right and lower left are repeated from Figure 2.

the March eruption results in a larger absolute change in insolation. Calculating the relative changes, the March eruption results in a peak value of 3% reduction in insolation, with the June eruption producing a 7% reduction, August eruption producing a 6% reduction, and December eruption producing a 2% reduction. This helps explain the larger in magnitude radiative forcing for the June eruption than the March eruption. The December eruption shows very little insolation reduction due to the low amount of sunlight at the latitudes where the aerosol layer resides.

[17] Integrating the values of radiative forcing over the 4 year period covered by these simulations, the June ensemble shows the largest integrated radiative forcing. This motivates our choice of this particular ensemble in our later analysis of the model ocean. Although Figure 4 shows a higher peak of Northern Hemisphere averaged optical depth, Figure 5 shows a higher peak in the zonal average by approximately 25%. The June and August ensembles also show persistence of the aerosol layer into the early spring following the eruption, whereas the others do not. Figure 6 shows the latitudinal extent of the radiative forcing has a seasonal dependence. The June eruption shows the greatest incursion into the tropics and subtropics. Since tropical insolation does not have a large seasonal cycle, this must be due to differences in atmospheric transport of the aerosols. However, the values of radiative forcing in the tropics are so small that these incursions cause negligible effects.

[18] The rate of deposition of the aerosols plays an important role in determining the climate effects, as aerosols that stay in the atmosphere longer can perturb the radiative balance for a longer period of time. Figure 8 shows anomalous annual sulfate deposition rates for the 5 Tg injection ensembles. The deposition rates are given as 10^{-5} kg m^{-2} a^{-1}. For comparison, if the average 4° latitude by 5° longitude grid box is 400 km by 500 km, 10^{-5} kg m^{-2} a^{-1} over an entire grid box is approximately 2 kg a^{-1}. The highest deposition rates occur in the midlatitude storm tracks during the boreal spring and summer [*Kravitz et al.*, 2009, 2010b]. In the autumn and winter, the dominant means of deposition appears to be large-scale subsidence near 30°N. The peak deposition rates are similar in all parts of Figure 8, suggesting the rate is proportional to the amount of material. The slightly higher deposition rates for the 1 March ensemble help explain why peak optical depth in this ensemble is lower than the June and August injection ensembles.

4. Climate Effects

[19] Figure 9 shows line graphs of Northern Hemisphere averaged surface air temperature anomaly (volcano plus

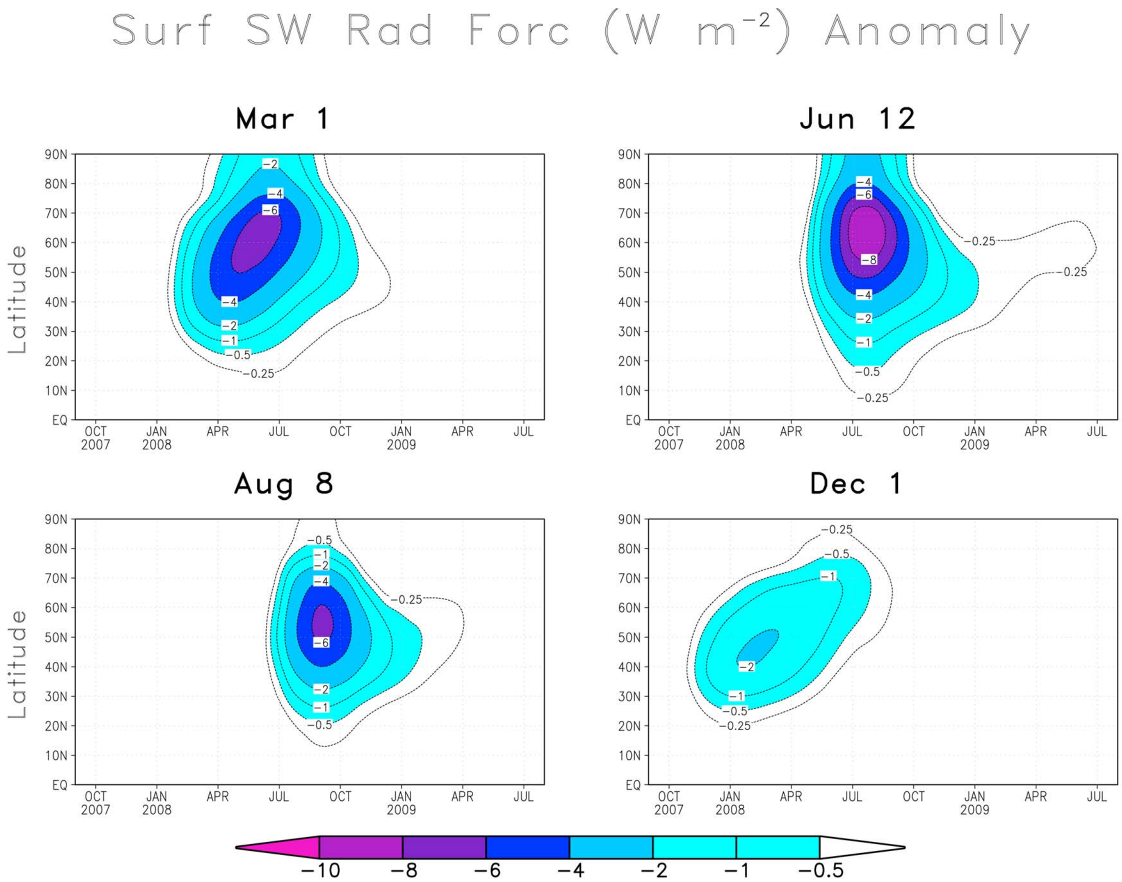

Figure 6. Zonally averaged surface shortwave radiative forcing (W m^{-2}) due to sulfate aerosols for the four 5 Tg injection ensembles. All ensembles pictured are averages of 20 model runs. Only the Northern Hemisphere is shown, as all values are zero in the Southern Hemisphere. Top right and lower left are repeated from Figure 3.

A1B ensemble minus A1B ensemble) and globally averaged precipitation anomaly for the June and August ensembles. For the 5 Tg eruptions, the June eruption shows a stronger decrease in temperature than the August eruption by nearly a factor of 2. Also, even a 3 Tg eruption in June shows more cooling than a 5 Tg eruption in August, strongly suggesting a confirmation of our hypothesis that the time of year of an eruption is critical in estimating climate impact. Moreover, there is very little difference between the climate impact of the 3 and 5 Tg August eruptions, which suggests the August eruptions are too late in the year to cause a climate impact. We do not detect any significant signal in globally averaged precipitation from any of the eruptions. This is not unreasonable, since not only does precipitation have a large natural variability, but for all simulations, the aerosols formed well after June, missing the chance to mitigate a large amount of summer continental heating. We also analyzed spatial maps of summer precipitation for these eruptions (not pictured) but found no patterns to suggest a reduction in the summer monsoon system. In contrast, the aerosols from the March injection would have been present during the monsoon period. However, due to the relatively low radiative forcing from this eruption, the temperature perturbations, as reported in Figure 10, do not show any large anomalies from this ensemble. Consequently, we would not expect a monsoonal disruption, and indeed, the precipitation results show no such anomalies. The December ensemble also shows nothing substantial, which we expect, due to the quite low optical depth and radiative forcing.

[20] To evaluate the statistical significance of the anomalies in Figures 9 and 10, we analyzed data provided by the National Climatic Data Center (NCDC) and the University of East Anglia's Climatic Research Unit (CRU). From NCDC, we obtained gridded data at 5° latitude by 5° longitude, created from version 2 of the Global Historical Climatology Network (GHCNv2) [*Free et al.*, 2004; *Peterson and Vose*, 1997; *Peterson et al.*, 1998]. From CRU, we obtained variance adjusted land air temperature anomalies, also gridded at 5° latitude by 5° longitude (CRUTEM3v) [*Brohan et al.*, 2006; *Jones et al.*, 1999; *Rayner et al.*, 2003, 2006].

[21] Calculations were performed based on a Student's t test with the number of degrees of freedom equal to the number of years in each of the sources' records, which is 130 for the NCDC GHCNv2 temperature record (1880–2009), 110 for the NCDC GHCNv2 precipitation record (1900–2009), and 160 for the CRUTEM3v temperature record (1850–2009). (We were unable to obtain precipitation data from CRU.) For an anomaly to be statistically significant at the 95% confidence level, it must be at least

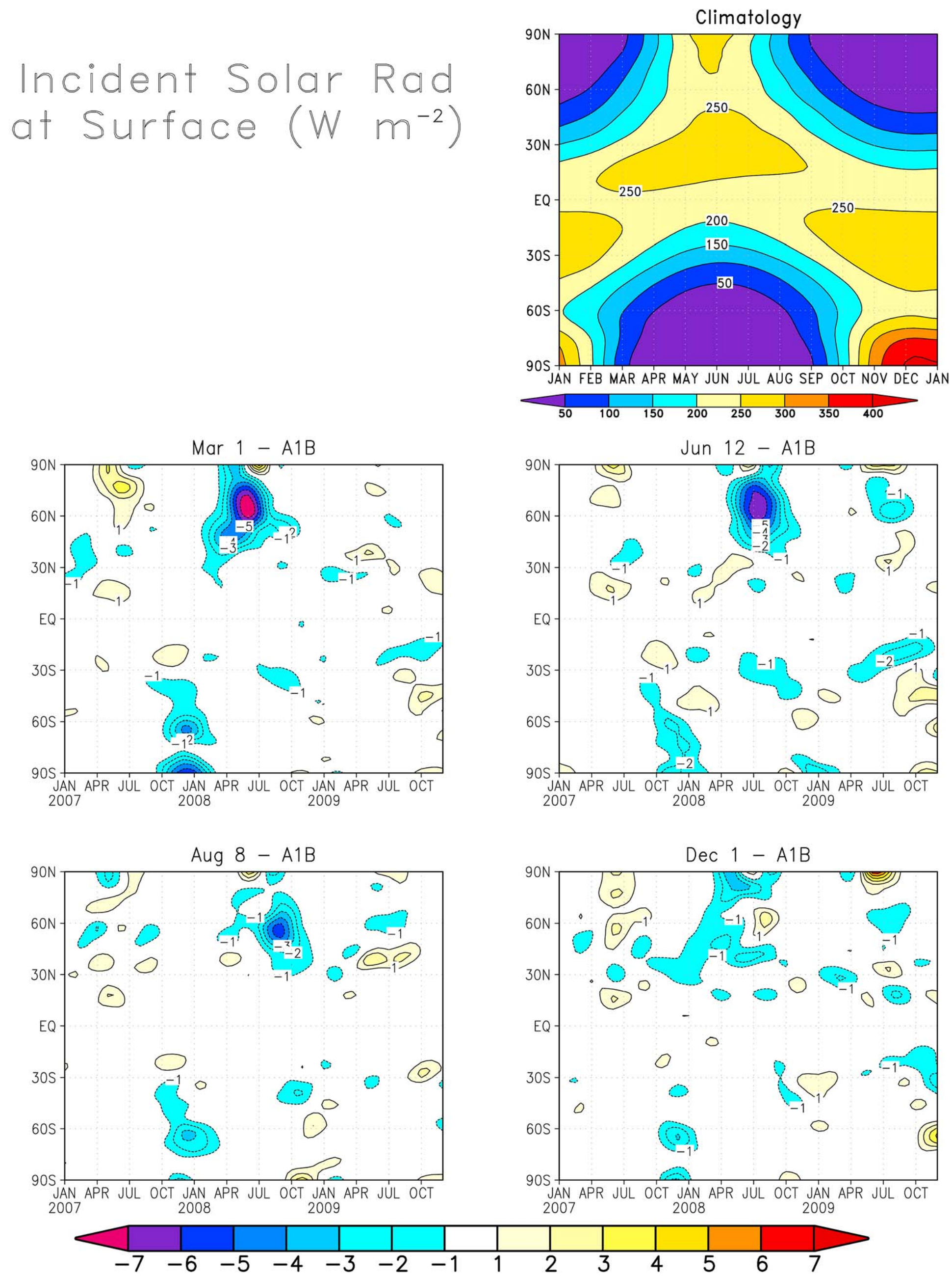

Figure 7. Incident solar radiation at the surface. (top) A zonal average climatology from a 183 year control run (constant 2007 conditions). (middle and bottom) Zonally averaged anomalies (volcano minus A1B) for the 5 Tg eruption ensembles (20 members each).

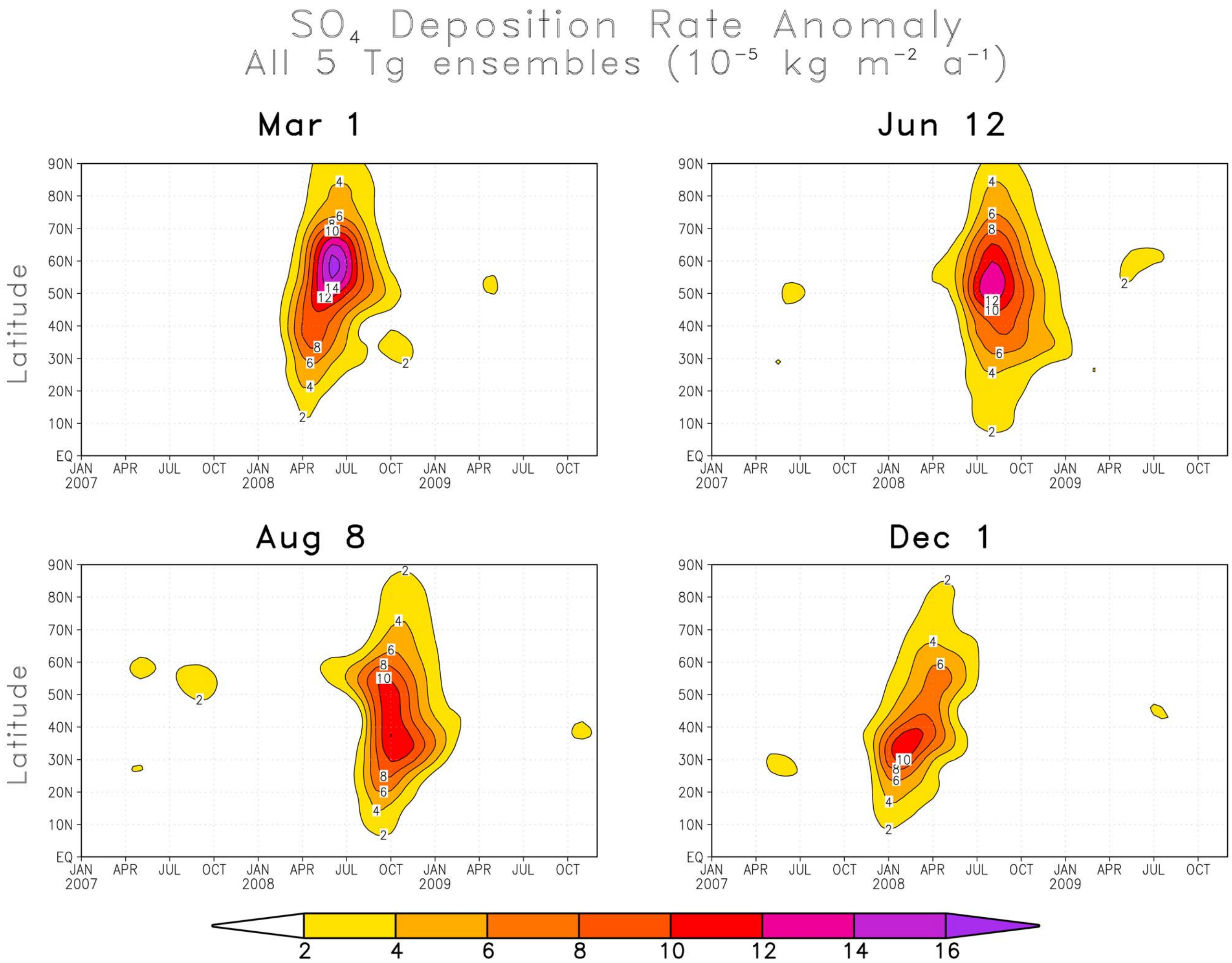

Figure 8. Sulfate deposition rates for the 5 Tg injection ensembles. Deposition rates show a strong seasonal dependence in both latitude and amount.

0.21°C different from a 12 month centered running mean ($t - 6$ months to $t + 5$ months) according to GHCNv2 data and at least 0.24°C according to CRUTEM3v data. To be significant at the 90% level, it must be 0.18°C or 0.20°C different from the 12 month running mean, respectively. The difference between the values for the two records is due to the number of degrees of freedom each record has. Precipitation must be 0.23 mm/d different from the 12 month running mean to be significant at the 95% level and 0.19 mm/d to be significant at the 90% level.

[22] For the values reported in Figure 9, only the 5 Tg eruption on 12 June has statistically significant anomalies according to the above criteria. For this ensemble, the September anomaly is 0.21°C lower than the 12 month running mean centered on that month, meaning it is statistically significant at the 90% confidence level according to both sets of data and at the 95% confidence level according to the GHCNv2 data. This is the only point of all ensembles that is statistically significant at the 90% level or better. No precipitation values are statistically significant at either the 90% or 95% confidence levels, and the actual anomaly values are approximately 1 order of magnitude below global average values needed to be considered significant. For Figure 10, again, only the June ensemble shows statistically significant results.

[23] We also compared our results with the natural variability in the climate model. The green lines in Figure 9 denote a climatology of the standard deviation of the A1B ensemble, and the yellow lines show the same for a 183 year control run of constant 2007 conditions. The 3 and 5 Tg June eruptions both show a statistically significant (~2σ) anomaly compared to the A1B climatology, as does the August 5 Tg ensemble, and the 5 Tg June ensemble is additionally statistically significant compared to the long control run. The March, June, and August 5 Tg ensembles are all statistically significant compared to the A1B climatology, but the June experiment is still the only ensemble which is significant according to the long control run. However, the March experiment shows an anomaly greater than 1σ of the long control run.

[24] These results reinforce current knowledge about the climate effects of large volcanic eruptions. Although a 5 Tg eruption in June does have detectable climate effects ac-

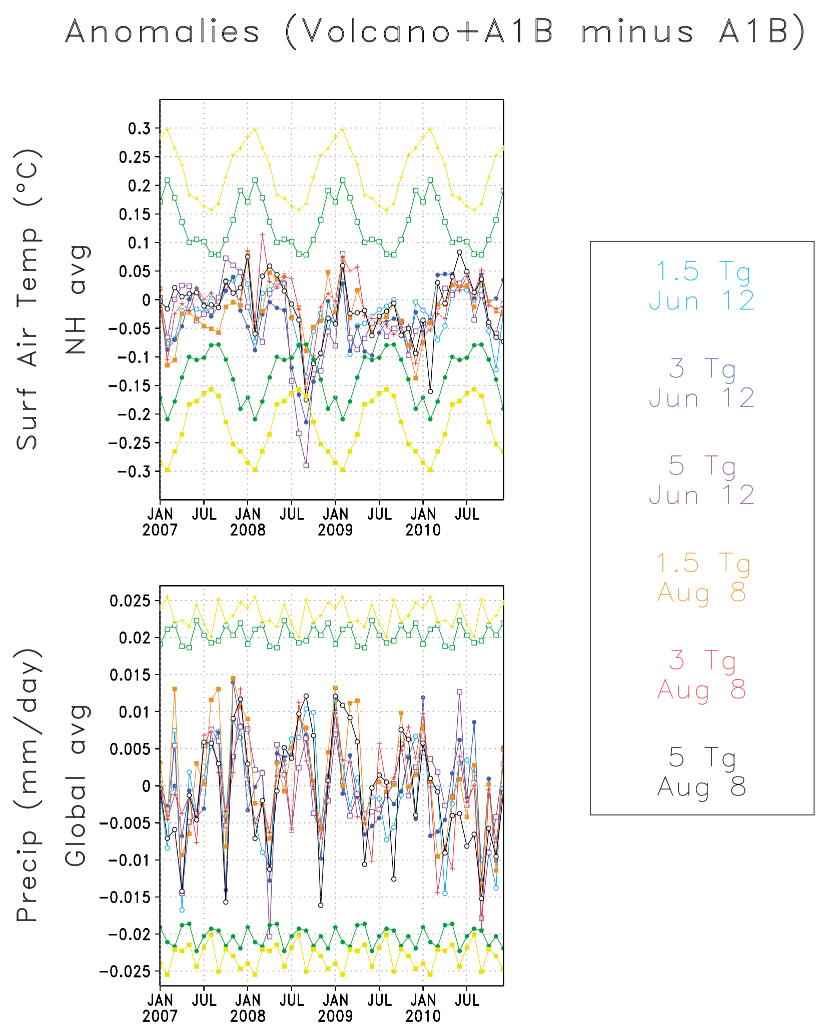

Figure 9. Line graphs of surface air temperature and precipitation anomalies due to the volcanic eruptions. Surface air temperature is averaged over the Northern Hemisphere to accentuate changes in temperature over Northern Hemisphere continents, and precipitation is globally averaged. All ensembles are averages of 20 model runs. The light green lines show the average seasonal cycle of the standard deviation from zero anomaly of the A1B runs as an indication of natural variability. The yellow lines show the same for a 183 year control run (constant 2007 conditions).

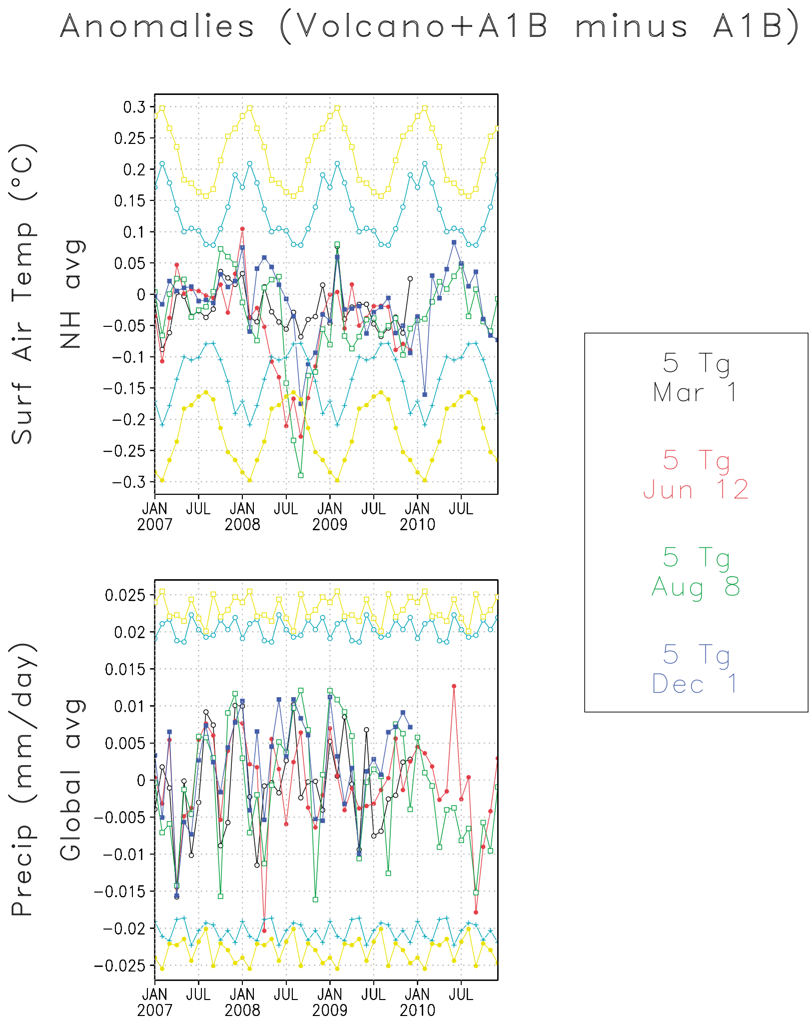

Figure 10. Same as Figure 9 for the 5 Tg ensembles (20 members each). The turquoise line shows a climatology of the standard deviation of the A1B ensemble, and the yellow line is a climatology of a 183 year control run (constant 2007 conditions).

cording to *Oman et al.* [2005], the effects of Katmai were found to be only barely distinguishable from weather noise. Moreover, not only is precipitation highly variable, hampering the ease by which an anomaly can be considered significant, but the aerosols would have completely formed well after June, so the first part of the monsoon, as well as the time period with the greatest amount of insolation, would be largely unaffected. Had the March eruption been larger, perhaps optical depth could have been sufficient in the summer to cause a monsoonal disruption. In contrast, a high-latitude eruption in the winter is significantly disadvantaged in causing climate effects. Assuming optical depth scales linearly with injection amount, which is a good assumption according to our results in Figures 1–3, for a December eruption to result in the same aerosol optical depth as a 5 Tg June eruption, the December eruption must inject at least 12 Tg of SO_2 into the lower stratosphere. However, there may be other factors at play should such a large eruption occur that we have not yet been able to investigate, and a high-latitude eruption of that magnitude has not been observed, hampering our ability to compare those results with data.

[25] After large tropical eruptions, such as the eruption of Mount Pinatubo in 1991, a positive mode of the Arctic Oscillation can result [*Stenchikov et al.*, 2002]. However, *Oman et al.* [2005] did not find any such evidence for the eruption of Katmai. We also analyzed various measurements of dynamics and circulation, including stratospheric height, sea level pressure, and zonal wind (not pictured). However, like *Oman et al.*, we did not find any significant perturbations. This leads us to conclude that high-latitude eruptions of the magnitudes we simulated would not cause significantly anomalous perturbations to circulation nor would they force a mode of the Arctic Oscillation.

5. Ocean Memory of Volcanic Eruptions

[26] For the calendar year (2009) after the 5 Tg eruption in June, the average Northern Hemisphere surface air temperature is 0.06°C lower than the calendar year before the eruption (2007). Although not statistically significant ac-

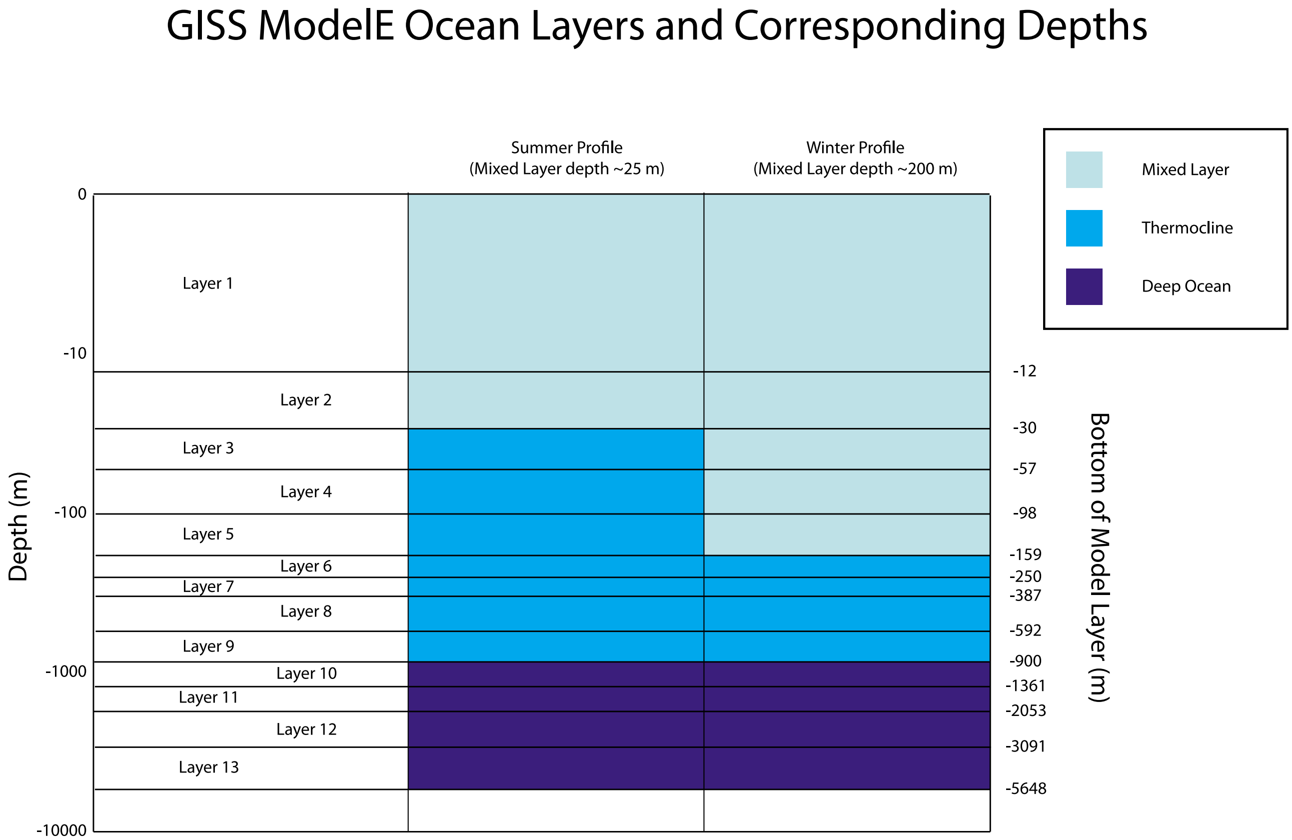

Figure 11. A diagram of the ocean layers in this version of ModelE [*Russell et al.*, 1995]. Model layer thicknesses do not adjust to topography and are either present in their entirety or absent. Determination of the ocean layer by depth follows guidelines by *de Boyer Montégut et al.* [2004], using a thermocline depth range of 25–1000 m in the summer and 200–1000 m in the winter (R. H. Stewart, Introduction to physical oceanography, 345 pp., 2007, available at http://oceanworld.tamu.edu/home/course_book.html).

cording to GHCNv2 or CRUTEM3v, this does pose the question as to why such a temperature pattern occurred. A natural explanation for this could be ocean memory of the cooling due to the eruption [*Stenchikov et al.*, 2009]. Although the version of the model we used to perform the simulations in this experiment does not provide us with enough information to assess changes in ocean heat content, we can still evaluate some oceanic changes.

[27] Figure 12 shows the ocean potential temperature anomaly for the top eight layers in the model's ocean for the 5 Tg 12 June eruption. Again, this ensemble was chosen because it shows the largest integrated radiative forcing anomaly, as calculated from Figure 4. The depths of the model's ocean layers are given in Figure 11. In the top five layers, we see a sharp, discontinuous cooling immediately after the volcanic eruption. Layers 1 and 2, which constitute the mixed layer at this time of year, show the largest drop. Despite technically being at the top of the thermocline according to *de Boyer Montégut et al.* [2004], we argue layer 3 is actually part of the mixed layer, due to its precipitous drop in temperature immediately after the volcanic eruption. Layers 4 and 5 also show a sharp drop, although not nearly as strongly as found in layers 1–3 and delayed several months after the drop in the upper layers, suggesting layers 4 and 5 are below the mixed layer. Layers 6 and 7 show a slight warming over the period affected by the volcano, but we were unable to determine a physical mechanism for this from the standard model output. Layer 8 shows little variability, suggesting the volcanic signal is not felt in the deep ocean during the time period represented in these simulations. Layers 1 and 2 return to zero anomaly only by the end of the simulation, and layers 3 and 4 still have not recovered to zero anomaly by this time. We expect the recovery of layers below the mixed layer to be slower, since these are much more removed from the atmospheric seasonal cycle than are the surface layers.

[28] To quantify these results, we calculated a climatology of the standard deviation of 100 years of a long control run (constant 2007 conditions), the results of which are shown in Figure 13. The model had not yet reached equilibrium by the end of this run, resulting in some amount of warming of the middle and deep ocean. This impacted the standard deviations of layers 7 and 8, so we are unable to reliably make assessments of the statistical significance of temperature anomalies in these layers. Comparing these results to the values in Figure 12, although none of the anomalies given is significant at the 95% confidence level, several of the large changes in ocean potential temperature are. Layer 1 anomaly drops from 0.04°C prior to the eruption to −0.05°C after the eruption (peak value), which is a statistically sig-

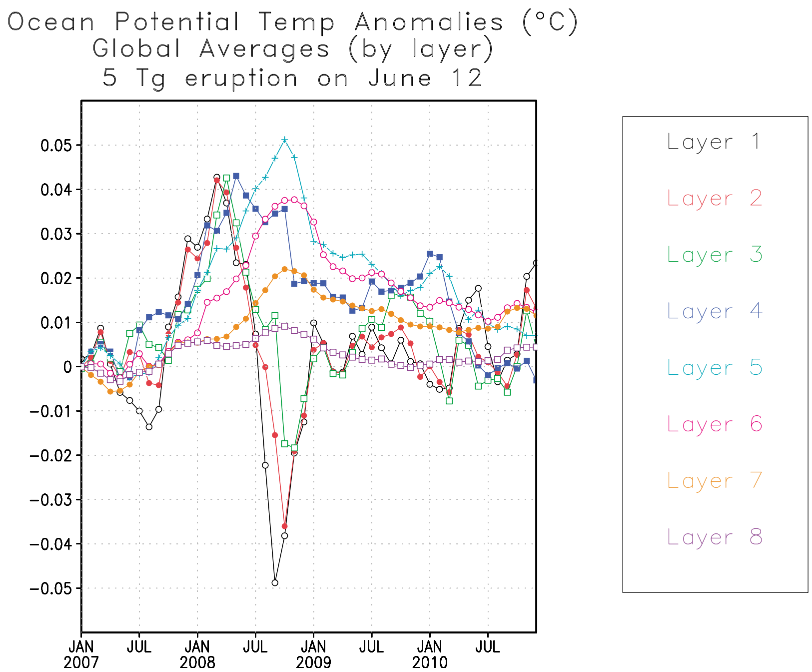

Figure 12. Global average of ocean potential temperature anomaly in the 5 Tg eruption on 12 June for the top 8 layers (out of 13) in the model. Thicknesses and depths of the layers are given in Figure 11. Layers 1–3 constitute the mixed layer at the time of the eruption, and layers 4–9 constitute the thermocline. Statistical significance of these values can be determined by comparison with the values given in Figure 13.

nificant change according to the values in Figure 14. Layer 2 drops from 0.04°C to −0.04°C, and layer 3 drops from 0.04°C to −0.02°C, both of which are statistically significant changes. The sharp drop in layer 4 has magnitude approximately 0.025°C, which is not statistically significant but is still apparent as a sharp drop. Below this layer, the changes are too subtle to specifically attribute them to a response to a large radiative forcing, and any changes are below the statistical significance threshold. From this, we conclude the mixed layer likely shows a measurable response in ocean temperature to the volcanic eruption. Qualitatively, the upper thermocline also shows a response, although we cannot draw any firm conclusions to support this (Figure 13).

6. Comparison to Katmai

[29] We compared our climate simulations to the observed effects of the eruption of Katmai (Novarupta) Volcano (58.3°N, 155.0°W) on 6 June 1912, which injected 5 Tg of SO_2 into the lower stratosphere. Katmai was known to have climate effects, including cooling over Northern Hemisphere continents in the summer of the eruption and a weakening of the Indian-African monsoon system, as was evidenced by low river flow in those areas [*Oman et al.*, 2005]. In this section, we compare our results with those of *Oman et al.*, who performed simulations of Katmai with a very similar setup of the same model.

[30] The simulations performed by *Oman et al.* [2005] involved two ensembles. The control ensemble was composed of 10 model runs at constant greenhouse gas and aerosol concentrations and was then time-averaged to produce a 40-member ensemble. The volcano ensemble was an average of 20 runs using the same conditions as the control runs, but involving specified aerosol optical depths from *Ammann et al.* [2003], corrected to have a variable aerosol effective radius, as in the work of *Sato et al.* [1993], which is in good agreement with *Stothers* [1997]. This is in contrast to our simulations, in which sulfate aerosol formation was calculated in the model. We also used a fully dynamic ocean, whereas *Oman et al.* used fixed sea surface temperatures and sea ice conditions prescribed by a 1946–1955 average [*Rayner et al.*, 2003].

[31] Figure 14 shows plots of surface air temperature anomaly due to a 5 Tg eruption on 12 June 2008, compared to the same results for simulations of the eruption of Katmai. We only show plots for surface air temperature, as Figures 9 and 10 suggest our plots of precipitation will show no significant results (which indeed they do not; not pictured), and *Oman et al.* [2005] similarly do not include plots of precipitation for their simulations of Katmai. Both sets of simulations show very similar patterns for the summer of the eruption (JJA), including a general pattern of cooling over the Northern Hemisphere continents, and the winter after the eruption (DJF) in the form of warming over the Northern Hemisphere continents.

[32] However, the patterns that appear in the simulations of Katmai are generally stronger and more pronounced than the anomalies in our simulations. We suggest several reasons for this discrepancy. First, we would not expect the patterns to be identical, since our aerosols are formed by the model and interact with the circulation, whereas the aerosols

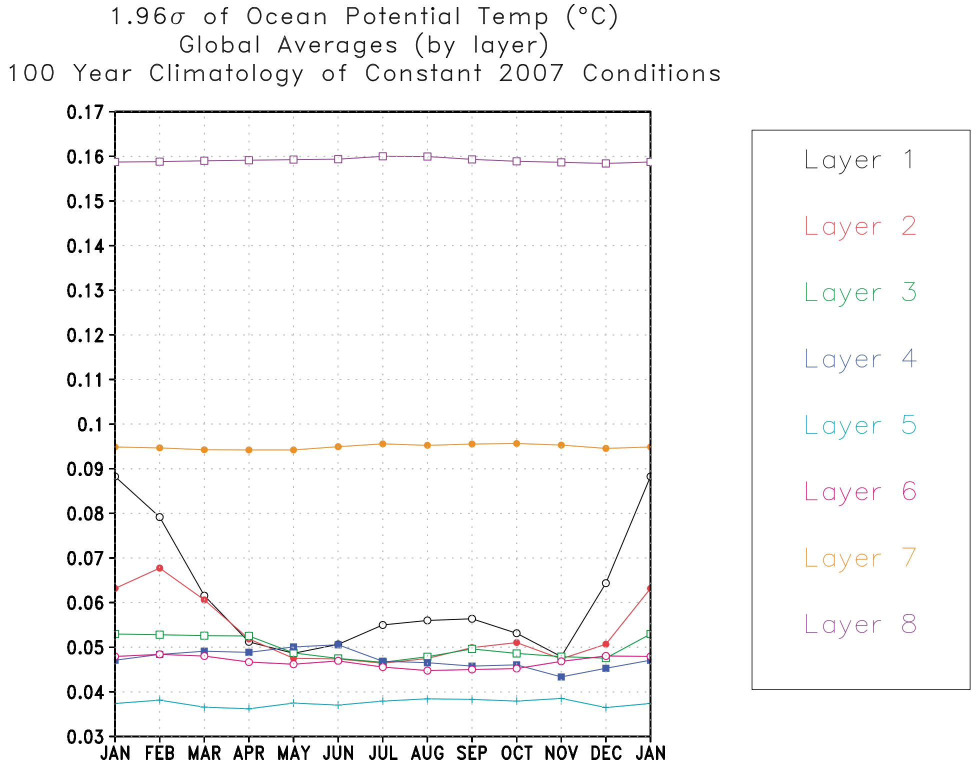

Figure 13. Climatology of 1.96 standard deviations of ocean potential temperature for ocean layers 1–8 in the model. Standard deviation was calculated over 100 years as anomalies from the mean of a control run (constant 2007 conditions). Layers 7 and 8 show comparatively large standard deviations from slow accumulation of heat in the deep ocean due to insufficient time allowed for model spin-up.

in the Katmai simulations do not. Our peak values of aerosol optical depth are consistent with those of *Oman et al.* (0.3 in September after the eruption). Moreover, fixed sea surface temperatures would negate the ocean memory effect seen in Figure 12, and using fixed sea surface temperatures can amplify surface air temperature anomalies, offering an additional explanation for the larger anomalies in the Katmai simulations [*Hansen et al.*, 2005]. Additionally, *Oman et al.* performed their statistical tests differently, using a single sample Student's *t* test based on 40 years of control runs. We used an unpaired two sample Student's *t* test based on 20 runs each. This difference in calculations appears to have the effect of making more of their results statistically significant than ours, given similar levels of anomaly.

7. Relevance to Stratospheric Geoengineering

[33] Several past studies have investigated Arctic geoengineering [e.g., *Caldeira and Wood*, 2008; *Robock et al.*, 2008] as a means of reducing the amount of direct interference in the climate system when compared to tropical geoengineering. Large injections of sulfur into the stratosphere at Northern Hemisphere high latitudes would result in an aerosol layer that cooled the Northern Hemisphere continents and prevented melting of the Arctic sea ice [*Robock et al.*, 2008]. The amount of sulfur needed would be less than in the case of a tropical injection, since the aerosols would not be distributed to the Southern Hemisphere, making this idea attractive to those who wish to consider injection of as little sulfur as possible.

[34] This study shows that in considering this type of geoengineering, the time of year of the injection is equally important to, if not more important than, the amount being injected. For example, most past geoengineering simulation has considered daily injections of SO_2 year-round. However, our study suggests injections in the winter are much less radiatively efficient than injections during the summer. Therefore, optimal geoengineering at high latitudes would only need to be done for part of the year. However, as we see from the March ensemble, one does not want to begin injections too early, as the radiative efficiency is still rather low.

[35] A natural consequence of these results would be to perform model simulations of Arctic geoengineering in the boreal spring, ceasing injections of SO_2 for the rest of the year. Not only would this be less invasive than year-round injections, but it would also take advantage of our findings. We caution any modeling groups conducting such simulations to ensure the amount of SO_2 they inject is of sufficient quantity to cause measurable surface cooling. However, we believe our findings should strongly discourage real-world testing of Arctic geoengineering, regardless of the time of year. *Oman et al.* [2005] and *Robock et al.* [2008] clearly show that any forcing from the aerosols that reduced surface temperatures would also weaken the monsoon system as a dynamical consequence. Moreover, to observe the results at

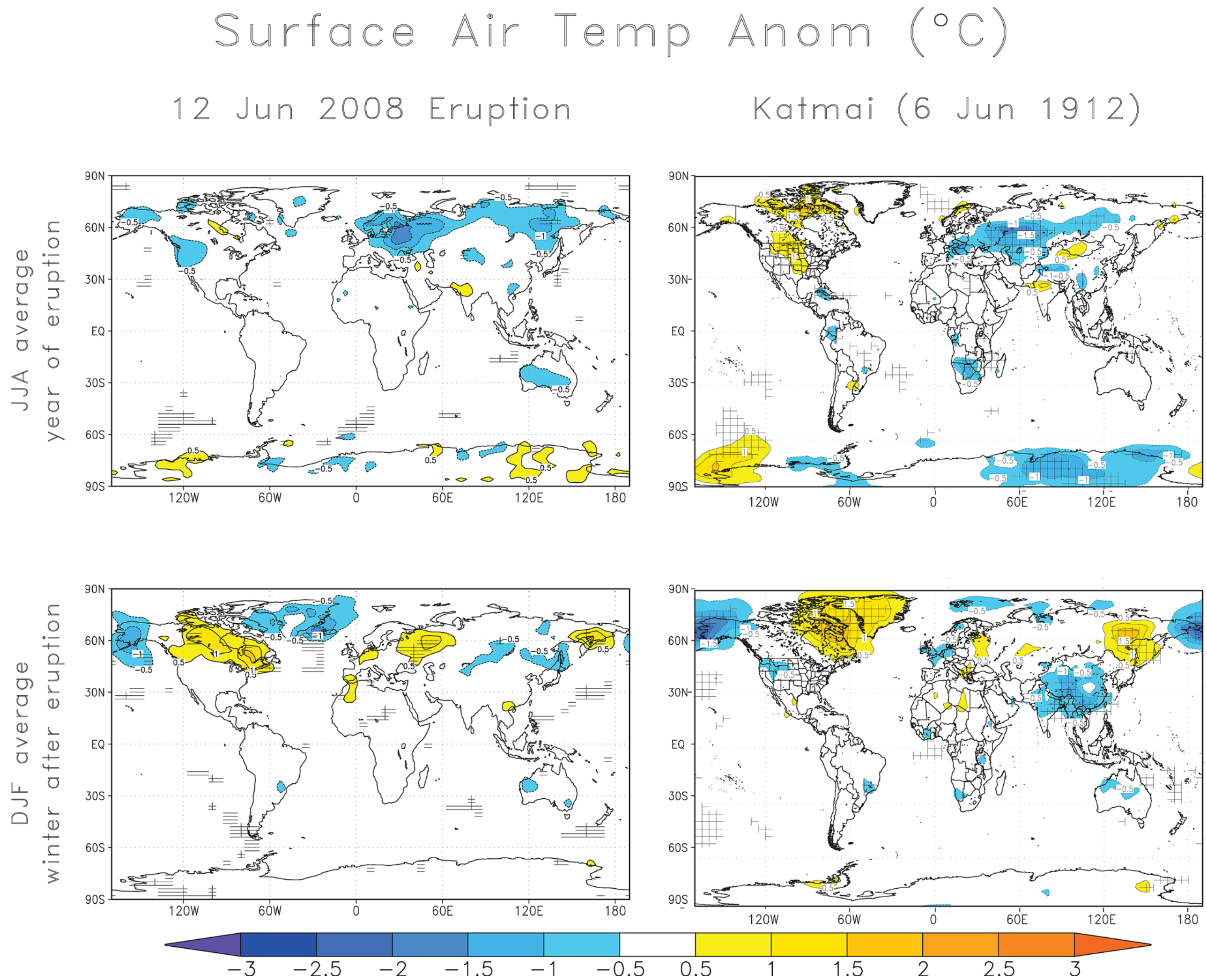

Figure 14. A comparison between simulations of (left) the 5 Tg eruption on 12 June 2008 and (right) simulations of Katmai from *Oman et al.* [2005] (reproductions of Figures 7a and 10a of *Oman et al.* [2005]). Statistical significance at the 95% confidence level is denoted by black hatching.

a satisfactory level of statistical significance, geoengineering would need to be conducted for a long period of time [*Robock et al.*, 2010]. Indeed, our simulations were conducted with 20 ensemble members, and our results were barely statistically significant, indicating that observing test results of geoengineering at the same level of certainty would require deployment for at least 20 years, which is quite a long period of time over which side effects will be felt.

8. Conclusions

[36] On the basis of our climate modeling study, the time of year of a high-latitude volcanic eruption is critical for determining the resulting climate effects, provided the eruption is large enough. Of the magnitudes we have investigated, a summer eruption was the only one that caused climate effects at a sufficient level of statistical significance. Extrapolating our results, a high-latitude eruption will have larger climate effects if it occurs in the summer, and it is unlikely to have climate effects if it erupts in the winter, unless the eruption is particularly large. Regardless of the time of year, a high-latitude eruption of the magnitudes we have simulated would not likely cause significant dynamical perturbations or change the general circulation.

[37] In line with *Stenchikov et al.* [2009], we further conclude the ocean has memory of the cooling an eruption causes, which can serve to modulate changes in climate. However, the runs we have completed are not long enough to fully assess the impacts of the ocean on the climate system. We stress that simulations of large eruptions need to include a complex ocean to capture these potentially important effects.

[38] From our results, the optimal time for an eruption to have the largest climate effects appears to be late spring to early summer. This study also prompts several additional questions. One such question is what are the dominant parameters that determine whether an eruption will have climate effects? It appears the summer eruption is an ideal or near-ideal combination of aerosol formation rate, deposi-

tion, and insolation. Conducting further simulations while artificially varying these parameters could be useful in determining the dominant effects. Additionally, we could ask how the details under which we run our simulations affect our results. Our comparison with Katmai could benefit from determination of the individual effect of prescribed optical depth versus being dynamically linked to stratospheric circulation and the effect of using fixed sea surface temperatures versus a dynamic ocean.

[39] **Acknowledgments.** We thank the reviewers for their helpful comments and suggested improvements to the paper. Model development and computer time at Goddard Institute for Space Studies are supported by National Aeronautics and Space Administration climate modeling grants. This work is supported by NSF grant ATM-0730452.

References

Ammann, C. M., G. A. Meehl, W. M. Washington, and C. S. Zender (2003), A monthly and latitudinally varying volcanic forcing data set in simulations of 20th century climate, *Geophys. Res. Lett.*, *30*(12), 1657, doi:10.1029/2003GL016875.

Brohan, P., J. J. Kennedy, I. Harris, S. F. B. Tett, and P. D. Jones (2006), Uncertainty estimates in regional and global observed temperature changes: A new data set from 1850, *J. Geophys. Res.*, *111*, D12106, doi:10.1029/2005JD006548.

Budyko, M. I. (1977), *Climatic Changes*, 261 pp., AGU, Washington, D. C.

Caldeira, K., and L. Wood (2008), Global and Arctic climate engineering: Numerical model studies, *Philos. Trans. R. Soc., Ser. A.*, *366*, 4039–4056, doi:10.1098/rsta.2008.0132.

Corradini, S., L. Merucci, A. J. Prata, and A. Piscini (2010), Volcanic ash and SO_2 in the Kasatochi and Okmok eruptions: Retrievals from different IR satellite sensors, *J. Geophys. Res.*, *115*, D00L21, doi:10.1029/2009JD013634.

de Boyer Montégut, C., G. Madec, A. S. Fischer, A. Lazar, and D. Iudicone (2004), Mixed layer depth over the global ocean: An examination of profile data and a profile-based climatology, *J. Geophys. Res.*, *109*, C12003, doi:10.1029/2004JC002378.

Free, M., J. K. Angell, I. Durre, J. Lanzante, T. C. Peterson, and D. J. Seidel (2004), Using first differences to reduce inhomogeneity in radiosonde temperature data sets, *J. Clim.*, *17*, 4171–4179, doi:10.1175/JCLI3198.1.

Hansen, J., et al. (2005), Efficacy of climate forcings, *J. Geophys. Res.*, *110*, D18104, doi:10.1029/2005JD005776.

Haywood, J., et al. (2010), Observations of the eruption of the Sarychev volcano and simulations using the HadGEM2 climate model, *J. Geophys. Res.*, *115*, D21212, doi:10.1029/2010JD014447.

Intergovernmental Panel on Climate Change (IPCC) (2001), *Climate Change 2001: The Scientific Basis, Contribution of Working Group I to 1006 the Third Assessment Report of the Intergovernmental Panel on Climate Change*, edited by J. T. Houghton et al., Cambridge Univ. Press, Cambridge, UK.

Intergovernmental Panel on Climate Change (IPCC) (2007), *Climate Change 2007: The Physical Science Basis. Contribution of Working Group I to the Fourth Assessment Report of the Intergovernmental Panel on Climate Change*, edited by S. Solomon et al., Cambridge Univ. Press, Cambridge, UK.

Jones, P. D., M. New, D. E. Parker, S. Martin, and I. G. Rigor (1999), Surface air temperature and its variations over the last 150 years, *Rev. Geophys.*, *37*(2), 173–199, doi:10.1029/1999RG900002.

Koch, D., G. A. Schmidt, and C. V. Field (2006), Sulfur, sea salt, and radionuclide aerosols in GISS ModelE, *J. Geophys. Res.*, *111*, D06206, doi:10.1029/2004JD005550.

Kravitz, B., A. Robock, L. Oman, G. Stenchikov, and A. B. Marquardt (2009), Sulfuric acid deposition from stratospheric geoengineering with sulfate aerosols, *J. Geophys. Res.*, *114*, D14109, doi:10.1029/2009JD011918.

Kravitz, B., A. Robock, and A. Bourassa (2010a), Negligible climatic effects from the 2008 Okmok and Kasatochi volcanic eruptions, *J. Geophys. Res.*, *115*, D00L05, doi:10.1029/2009JD013525.

Kravitz, B., A. Robock, L. Oman, G. Stenchikov, and A. B. Marquardt (2010b), Correction to Sulfuric acid deposition from stratospheric geoengineering with sulfate aerosols, *J. Geophys. Res.*, *115*, D16119, doi:10.1029/2010JD014579.

Oman, L., A. Robock, G. L. Stenchikov, G. A. Schmidt, and R. Ruedy (2005), Climatic response to high-latitude volcanic eruptions, *J. Geophys. Res.*, *110*, D13103, doi:10.1029/2004JD005487.

Oman, L., A. Robock, G. L. Stenchikov, T. Thordarson, D. Koch, D. T. Shindell, and C. Gao (2006a), Modeling the distribution of the volcanic aerosol cloud from the 1783–1784 Laki eruption, *J. Geophys. Res.*, *111*, D12209, doi:10.1029/2005JD006899.

Oman, L., A. Robock, G. L. Stenchikov, and T. Thordarson (2006b), High-latitude eruptions cast shadow over the African monsoon and the flow of the Nile, *Geophys. Res. Lett.*, *33*, L18711, doi:10.1029/2006GL027665.

Peterson, T. C., and R. S. Vose (1997), An overview of the Global Historical Climatology Network temperature database, *Bull. Am. Meteorol. Soc.*, *78*, 2837–2849, doi:10.1175/1520-0477(1997)078<2837:AOOTGH>2.0.CO;2.

Peterson, T. C., T. R. Karl, P. F. Jamason, R. Knight, and D. R. Easterling (1998), The first difference method: Maximizing station density for the calculation of long-term global temperature change, *J. Geophys. Res.*, *103*(D20), 25,967–25,974, doi:10.1029/98JD01168.

Rayner, N. A., D. E. Parker, E. B. Horton, C. K. Folland, L. V. Alexander, D. P. Rowell, E. C. Kent, and A. Kaplan (2003), Globally complete analyses of sea surface temperature, sea ice, and night marine air temperature, 1871–2000, *J. Geophys. Res.*, *108*(D14), 4407, doi:10.1029/2002JD002670.

Rayner, N. A., P. Brohan, D. E. Parker, C. K. Folland, J. J. Kennedy, M. Vanicek, T. Ansell, and S. F. B. Tett (2006), Improved analyses of changes and uncertainties in marine temperature measured in situ since the mid-nineteenth century: The HadSST2 data set, *J. Clim.*, *19*, 446–469, doi:10.1175/JCLI3637.1.

Robock, A. (2000), Volcanic eruptions and climate, *Rev. Geophys.*, *38*(2), 191–219, doi:10.1029/1998RG000054.

Robock, A. (2003), Volcanoes: Role in climate, in *Encyclopedia of Atmospheric Sciences*, edited by J. Holton et al., pp. 2494–2500, Academic, London, doi:10.1016/B0-12-227090-8/00448-6.

Robock, A., T. Adams, M. Moore, L. Oman, and G. Stenchikov (2007), Southern hemisphere atmospheric circulation effects of the 1991 Mount Pinatubo eruption, *Geophys. Res. Lett.*, *34*, L23710, doi:10.1029/2007GL031403.

Robock, A., L. Oman, and G. Stenchikov (2008), Regional climate responses to geoengineering with tropical and Arctic SO_2 injections, *J. Geophys. Res.*, *113*, D16101, doi:10.1029/2008JD010050.

Robock, A., M. Bunzl, B. Kravitz, and G. Stenchikov (2010), A test for geoengineering?, *Science*, *327*(5965), 530–531, doi:10.1126/science.1186237.

Russell, G. L., J. R. Miller, and D. Rind (1995), A coupled atmosphere-ocean model for transient climate change, *Atmos. Ocean*, *33*, 683–730.

Sato, M., J. E. Hansen, M. P. McCormick, and J. B. Pollack (1993), Stratospheric aerosol optical depths, 1850–1990, *J. Geophys. Res.*, *98*(D12), 22,987–22,994, doi:10.1029/93JD02553.

Schmidt, G. A., et al. (2006), Present day atmospheric simulations using GISS ModelE: Comparison to in situ, satellite and reanalysis data, *J. Clim.*, *19*, 153–192, doi:10.1175/JCLI3612.1.

Stenchikov, G. L., I. Kirchner, A. Robock, H.-F. Graf, J. C. Antuña, R. G. Grainger, A. Lambert, and L. Thomason (1998), Radiative forcing from the 1991 Mount Pinatubo volcanic eruption, *J. Geophys. Res.*, *103*(D12), 13,837–13,857, doi:10.1029/98JD00693.

Stenchikov, G., A. Robock, V. Ramaswamy, M. D. Schwarzkopf, K. Hamilton, and S. Ramachandran (2002), Arctic Oscillation response to the 1991 Mount Pinatubo eruption: Effects of volcanic aerosols and ozone depletion, *J. Geophys. Res.*, *107*(D24), 4803, doi:10.1029/2002JD002090.

Stenchikov, G., K. Hamilton, A. Robock, V. Ramaswamy, and M. D. Schwarzkopf (2004), Arctic Oscillation response to the 1991 Pinatubo eruption in the SKYHI GCM with a realistic Quasi-Biennial Oscillation, *J. Geophys. Res.*, *109*, D03112, doi:10.1029/2003JD003699.

Stenchikov, G., T. L. Delworth, V. Ramaswamy, R. J. Stouffer, A. Wittenberg, and F. Zeng (2009), Volcanic signals in oceans, *J. Geophys. Res.*, *114*, D16104, doi:10.1029/2008JD011673.

Stothers, R. B. (1997), Stratospheric aerosol clouds due to very large volcanic eruptions of the early twentieth century: Effective particle sizes and conversion from pyrheliometric to visual optical depth, *J. Geophys. Res.*, *102*(D5), 6143–6151, doi:10.1029/96JD03985.

Tang, I. N. (1996), Chemical and size effects of hygroscopic aerosols on light scattering coefficients, *J. Geophys. Res.*, *101*(D14), 19,245–19,250, doi:10.1029/96JD03003.

Thordarson, T., and S. Self (2003), Atmospheric and environmental effects of the 1783–1784 Laki eruption: A review and reassessment, *J. Geophys. Res.*, *108*(D1), 4011, doi:10.1029/2001JD002042.

Trenberth, K. E., and A. Dai (2007), Effects of Mount Pinatubo volcanic eruption on the hydrological cycle as an analog of geoengineering, *Geophys. Res. Lett.*, *34*, L15702, doi:10.1029/2007GL030524.

B. Kravitz and A. Robock, Department of Environmental Sciences, Rutgers University, 14 College Farm Rd., New Brunswick, NJ 08901, USA. (benkravitz@envsci.rutgers.edu; robock@envsci.rutgers.edu)